Journal of Mines, Metals and Fuels, *71(11): 2191-2201; 2023. DOI: 10.18311/jmmf/2023/36272*

Print ISSN : 0022-2755

Journal of Mines, Metals and Fuels

Contents available at: *www.informaticsjournals.com/index.php/jmmf*

Aluminum Oxide (Al_2O_3) Nanoparticles as Thermal Enhancers in Phase Change Materials for Electronic Devices

S. P. Prashanth[1]*, Devendra Dandotiya[1,2], A. M. Surendrakumar[1], Ujwal Sharma[3] and Anand K. Joshi[1]

[1]Department of Mechanical Engineering, Presidency University, Bangalore - 560064, Karnataka, India; prashanth.sp@presidencyuniversity.in

[2]Advanced Technology Research Center, Presidency University, Bangalore - 560064, Karnataka, India

[3]Daimler India Commercial Vehicles Pvt. Ltd., Kanchipuram - 602105, Tamil Nadu, India

Abstract

Nano-enhanced phase change materials (Nano-PCMs) are emerging as pivotal solutions in electronic cooling, primarily attributed to their remarkable energy storage and release abilities within confined spaces. These Nano-PCMs amalgamate phase change materials with nanoscale Aluminum Oxide (Al_2O_3) particles, elevating their thermal performance. Al_2O_3 nanoparticles employ a heat-based energy absorption mechanism, capturing thermal energy during temperature elevations and relinquishing it during cooling phases. This sets Nano-PCMs apart from conventional PCMs, especially for electronic cooling applications. Nano-PCMs find extensive use in electronic devices and data centers, contributing significantly to enhanced energy efficiency and reduced cooling expenditures. The selection of specific PCMs and Al_2O_3 nanoparticles depends on the targeted application. This study employs a 3D simulation to scrutinize heat distribution in a PCM/Nano-PCM-based heat sink, subject to variable heat fluxes ranging from 6 to 10 kW/m², enabling a comprehensive evaluation of heat dissipation over time. The findings underscore the pivotal role of Al_2O_3 nanoparticles in enhancing the heat sink's performance. At 6 kW/m² input, Nano-PCMs without fins reduce charging time by 6%, 11%, and 51% for Al_2O_3 nanoparticle volume fractions (φ) of 1%, 2.5%, and 5% in comparison to Pure-PCM (φ = 0%). Nano-PCMs with fins exhibit remarkable charging time reductions of 85%, 87%, and 89% for φ values of 69%, 78%, and 89% at 6 kW/m². These results emphasize the superior heat transfer characteristics of Al_2O_3-infused Nano-PCMs, offering a compelling solution for efficient electronic cooling.

Keywords: *Aluminum Oxide, Phase Change Material, Nano Particles, Nano-Phase Change Material*

1.0 Introduction

Nano-enhanced Phase Change Materials (Nano-PCMs) are an optimistic technology for electronic cooling applications because of their ability to store and release large amounts of energy in a small volume[1]. Nano-PCMs are materials that are filled with nanoscale particles, such as carbon nanotubes, which act as energy reservoirs. These nanoscale particles can absorb a heat-based way of storing energy, when the surrounding temperature rises, and release it when the temperature drops. Nano-PCMs can store and release energy more efficiently than traditional PCMs, making them ideal for cooling applications[2]. Nano-PCMs have been used in a variety of electronic cooling applications, including laptops, tablets, and other consumer electronics. In addition,

**Author for correspondence*

Nano-PCMs can be used to reduce the temperature of data centers, resulting in increased energy efficiency and reduced cooling costs. Depending on the application, various PCMs and nanoparticles can be used for NePCM production. For instance, paraffin wax is a popular PCM because of its high latent heat of fusion and low cost, while carbon nanotubes or graphene oxide are popular choices for nanoparticles due to their excellent thermal conductivity[3-5]. Several studies have described the use of PCM in conjunction with nanoparticles including expanded graphite, paraffin, carbon nanotubes, aluminum oxide, and others in conjunction with heat sinks energy storage systems. Modeling and simulation techniques can be used to optimize the design of NEPCMs for specific applications. Computational models can be used to predict the thermal behavior of the material under different operating conditions and to optimize the nanoparticle concentration and size for maximum thermal performance.

In the RT-58 PCM, Bernardo *et al*.,[6] used 1% and 5% of Al_2O_3 concentrated nanoparticles in the LHTES system. The researcher found that nanoparticle addition greatly increased the performance of the system. To examine the impacts of distributed nanomaterials on the heat transfer efficiency of a shell and tube system, Mahdavi *et al*.,[7] built a computational model in which between the PCM tank and the HTF, the heat pipes were positioned as a bridge. They used nanomaterials, such as CuO, Cu, Ag, and Al_2O_3. Their results indicated that the phase change time is significantly shortened when heat pipes and nanomaterials are used together. They concluded that the utilization of nanoparticles boosted the performance of the ystem. To develop an LHTES system, Ghalambaz *et al*.,[8] used a combined procedure based on the finite element method and Taguchi optimization approach. They utilized GO and Cu and said that adding Cu nanoparticles to the ideal design of the LHTES system boosted the heat transmission rate by nearly 45% in comparison to the basic design.

This computational study's goal is to evaluate the thermal performance of PCM/NePCM in electronic cooling applications while taking into account heat fluxes produced by electronic systems ranging from 6 to 10 kW/m^2. To assess the integration of nanoparticles at various volume fractions, namely = 1%, 2.5%, and 5%, transient 3D numerical simulations have also been carried out.

2.0 Numerical Modelling

In the current study, Pandiyan *et al*.,[9] experimental work is numerically simulated to evaluate the PCM's thermal properties for an application involving electronic cooling. Ansys fluent 16.2 software was used to change input parameters.

2.1 Problem's Physics

Based on the experimental results, a three-dimensional heat sink model has been taken into consideration. A

Table 1. Thermo-physical properties

Property	PCM	Nanomaterial Al_2O_3
Solid/Liquid temperature (K)	316/317	-
Thermal conductivity (W/m K)	0.15	40
Specific heat (kJ/kg K)	2.71	0.765
Dynamic viscosity (Pa-s)	0.0235	
Solidus/Liquid density (kg/m^3)	863/903	3970
Liquid specific heat (kJ/kg K)	2.78	-
Latent heat of fusion (kJ/kg)	199	-
Thermal coefficient expansion (K^{-1})	0.0001	

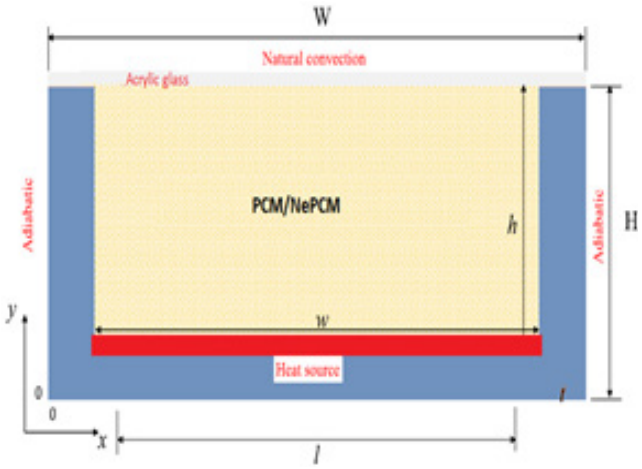

Figure 1. An illustration of the boundary conditions employed in the current investigation.

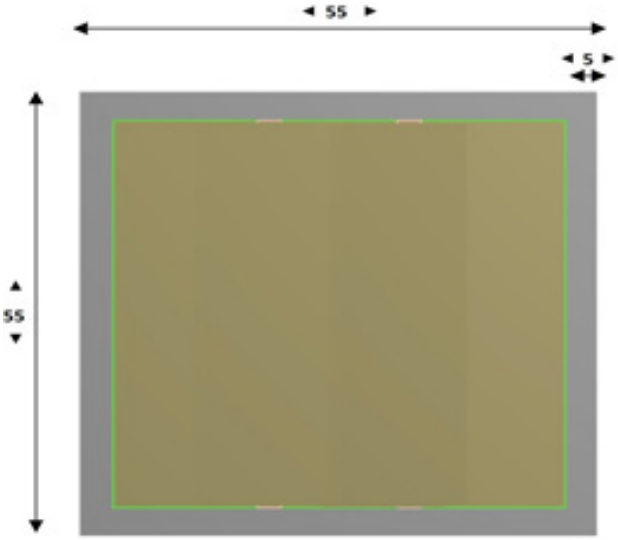

Figure 2. PCM container's top view, displaying the heat sink dimensions with fin in millimeters[9].

5mm thick acrylic plate serves as the rectangular heat sink's material. Table 1 lists the characteristics of the PCM and Nanoparticles utilized. In use, rubber insulation keeps heat from escaping the domain's bottom and top. Figure 1 depicts the diagram of the physical domain, which is the focus of this paper. The system considers the 3-D geometry of the heat sink with adiabatic and convective boundaries as well as input heat flux at the bottom of the sink. The dimensions of the heat sink are shown in Figure 2.

2.2 Governing Equations

Based on the problem under research, boundary conditions are expressed as indicated in Figure 1. To analyze the phase change in the PCM-based heat sink, the enthalpy-porosity data is used. To resolve the phase transition issue using the "melting and solidification" paradigm, below mentioned assumptions are made:

1. The melt is laminar, unsteady, and incompressible.
2. The heat sink's material is homogeneous and isotropic.
3. Between fins and liquid PCM local thermal equilibrium exists.
4. PCM and fin's thermophysical characteristics do not change with temperature or phase.
5. Viscous dissipation is considered negligible.
6. Minimal radiative heat transfer occurs.

2.2.1 Continuity Equation

$$\frac{\partial \rho}{\partial t} + \nabla.(\rho \vec{v}) = 0 \quad (1)$$

2.2.2 Momentum Equation

$$\frac{\partial}{\partial t}(\rho \vec{v}) + \nabla.(\rho \vec{v}\vec{v}) = -\nabla p + \nabla.(\bar{\bar{\tau}}) + \rho \vec{g} + \vec{F} + S \quad (2)$$

Where $\rho \vec{g}$ and $\vec{F}$ represent gravitational and external body forces, p is the static pressure, and $\bar{\bar{\tau}}$ is the stress tensor.

2.2.3 Equation of Energy

Enthalpy, H, is:

$$H = h + \Delta H \quad (3)$$

Sensible enthalpy is:

$$h = h_{ref} + \int_{T_{ref}}^{T} c_p dT \quad (4)$$

Where c_p represents specific heat at constant pressure. represents reference enthalpy of reference temperature T_{ref}.

During temperature, $T_{liquidus} > T > T_{solidus}$, the fraction of liquid occurs during the phase shift and ΔH represents latent heat content expressed as:

$$\gamma = \Delta H / L \quad (5)$$

$$= \begin{cases} 0, & if\ T < T_{solidus} \\ 1, & if\ T > T_{liquidus} \\ \dfrac{T - T_{solidus}}{(T_{liquidus} - T_{solidus})}, & if\ T_{liquidus} > T > T_{solidus} \end{cases} \quad (6)$$

The form of the energy equation for the solidification/melting problem is

$$\frac{\partial}{\partial t}(\rho H) + \nabla.(\rho \vec{v} H) = \nabla.(k \nabla T) + S \quad (7)$$

Where H, ρ, k, T and S represents enthalpy, density, thermal conductivity, temperature, and source term respectively.

In the momentum equation, Eq. (3), the source term S is

$$S = \frac{(1-\gamma)^2}{(\gamma^3 + \varepsilon)} A_{mush}(\vec{v} - \vec{v}_p) \quad (8)$$

Where $\frac{(1-\gamma)^2}{(\gamma^3 + \varepsilon)} A_{mush}(\vec{v} - \vec{v}_p)$ is the function of porosity,[10] used to "imitate" the equations of momentum for porous medium flow, which fulfills the basic idea to gradually decrease the velocities changing the phase. The mushy zone constant, A_{mush}, reflects its morphology, whose constant varies between 104 to 107, which matches the current model; It details how quickly the velocity goes down to zero as the substance solidifies. The ε is too small to avoid zero division (0.001)[11].

Based on the enthalpy porosity technique, the solidification-melting model in Fluent 16.2 software solidifies and melts and does not explicitly track the melt percentage. Three separate zones will be present when studying the phase transition of PCM: a zone of solid dendrites, a region of entire liquid, and a mushy region composed of liquid strewn among solid dendrites. The technique considers the requirement that all velocities in solid zones be zero by suitably specifying parameter A in Eqs (8). As the substance solidifies, the "pseudo-" porous medium that symbolizes the mushy zone has porosity values that range from 1 to 0. When the substance has completely solidified in a cell, the porosity drops to zero, which results in the velocities falling to zero[12].

Boussinesq approximation is considered for buoyancy-driven fluid flow considering temperature variation. A shortcode is interpreted in Ansys Fluent 16.2 to enable density variation for solid-to-liquid PCM.

2.3 Thermo-Physical Properties of NePCM

The thermo-physical characteristics of Pure-PCM are changed by adding Al_2O_3 nanoparticles. Differential scanning calorimetry, an expensive and time-consuming experimental technique, is required for the precise calculation of NePCM's thermophysical parameters (DSC). Alternatives for determining the effects of adding nanomaterials on its properties are experimental correlations and analytical models. Models of mixing by Pak and Cho[13], were able to accurately compute the thermos-physical characteristics of the NePCM, including density, specific heat, thermal expansion, and latent heat. Moreover, Vajjha *et al.*,[14] and Krieger and Dougherty,[15] also created several models that precisely predicted the viscosity of PCMs increased by nanotechnology. In the current investigation, the specific heat (C_p)/density (ρ) was computed using the mixing model as follows:

$$\rho_{NePCM} = (1-\varphi)\rho_{PCM} + \varphi\rho_{NM} \quad (9)$$

$$(\rho C_p)_{NePCM} = (1-\varphi)(\rho C_p)_{PCM} + \varphi(\rho C_p)_{NM} \quad (10)$$

$$(\rho L)_{NePCM} = (1-\varphi)(\rho L)_{PCM} \quad (11)$$

$$(\rho\beta)_{NePCM} = (1-\varphi)(\rho\beta)_{PCM} \quad (12)$$

The dynamic viscosity (μ) of NePCM must be estimated with the utmost accuracy since it acts as a powerful melting acceleration mechanism on natural convection. According to the type of nanomaterials used, three different models were used for this aim. The models of Vajjha *et al.*[14] compute the effective dynamic viscosity of the NePCM containing Al_2O_3 as follows:

$$\mu_{NePCM} = 0.983e^{(12.959\varphi)}\mu_{PCM} \quad (13)$$

An (intrinsic viscosity) value was taken to be 2.5 and ϕ *max* (maximum packing factor) was taken as 0.632 based on the shape of nanomaterials[13,15,17].

The thermal conduciveness of the NePCM was calculated using the Maxwell model,[18] for evenly sized spherical nanoparticles (metals and metal oxides), as stated in Eq. (14)

$$k_{NePCM} = k_{PCM}[\frac{k_{NP} + 2k_{PCM} - 2\varphi(k_{PCM} - k_{NP})}{k_{NP} + 2k_{PCM} + \varphi(k_{PCM} - k_{NP})} \quad (14)$$

2.4 Initial and Boundary Conditions

The PCM is solid at a temperature of 300 K. To the bottom wall of the heat sink input heat flux is provided, side walls are adiabatic, and the top surface of the heat sink is provided with a convection heat transfer rate of 5 kW/m^2. Referring to the research done by Ali *et al.*[19,20] and Arshad *et al.*[21,22] the boundary conditions are considered as follows:

1. Initial conditions

$t = 0, T = T_{ini} = 296.15$ K, $f_l = 0$

2. Boundary conditions

a. No-slip condition at walls: $u = v = 0$

b. Adiabatic walls:

$$-k\left.\frac{\partial T}{\partial x}\right|_{x=0,W} = 0 \qquad \text{Along vertical walls}$$

$$-k\left.\frac{\partial T}{\partial y}\right|_{\substack{x=0-5,45-55\\y=0}} = 0 \qquad \text{At the bottom surface}$$

c. Natural convection:

$$-k\left.\frac{\partial T}{\partial y}\right|_{y=H} = h(T - T_\infty)$$

d. Volumetric heat generation provided from heat source:

$$-k\left.\frac{\partial T}{\partial y}\right|_{\substack{x=5-45\\y=0-5}} = q'''$$

2.5 Transient Simulation Validation

The experimental findings from the PCM-based heat sink[9], are utilized to validate the current model. Figure 3, depicts numerical and experimental temperature results of the heat sink. Both numerical and experimental results are in good accord with each other with ±4% temperature difference, demonstrating the viability of using the current numerical model for future simulations. The PRESTO method is utilized to solve the pressure-correction equation; Pressure-velocity coupling is solved via the Pressure Implicit with Splitting of Operator (PISO) algorithm. Pressure, velocity, energy, and liquid fraction have relaxation value factors of 0.75, 0.75, 1, and 0.3, respectively.

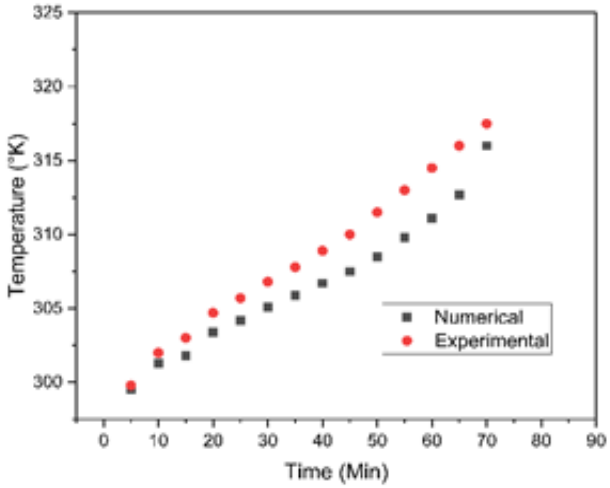

Figure 3. Numerical validation against experimental results.

2.6 Grid and Time-Step Independence Test

Time and grid independence experiments were conducted for heat sinks without fins at an input heat flux of 6 kW/m^2 to counterbalance the influence on numerical precision. During the grid independence test, three different mesh sizes with element sizes 39626, 78973, and 117456 were considered. Figure 4 displays the outcomes of liquid-fraction to each element's size. The greatest temperature differences were found to be 2.78 percent and 3.54 percent, respectively. The results demonstrate that no discernible change in the temperature distribution was observed for different time-step sizes. Based on the results, the mesh and time step size for the additional simulations in the current study were determined to be 78973 elements and t = 1s, respectively.

3.0 Results and Discussions

For PCM/NePCM, 3-D numerical simulations were run at five different heat fluxes (6, 7, 8, 9, and 10 kW/m^2). The charging procedure starts with supplying the heater's surface with a steady heat flux. Convection heat

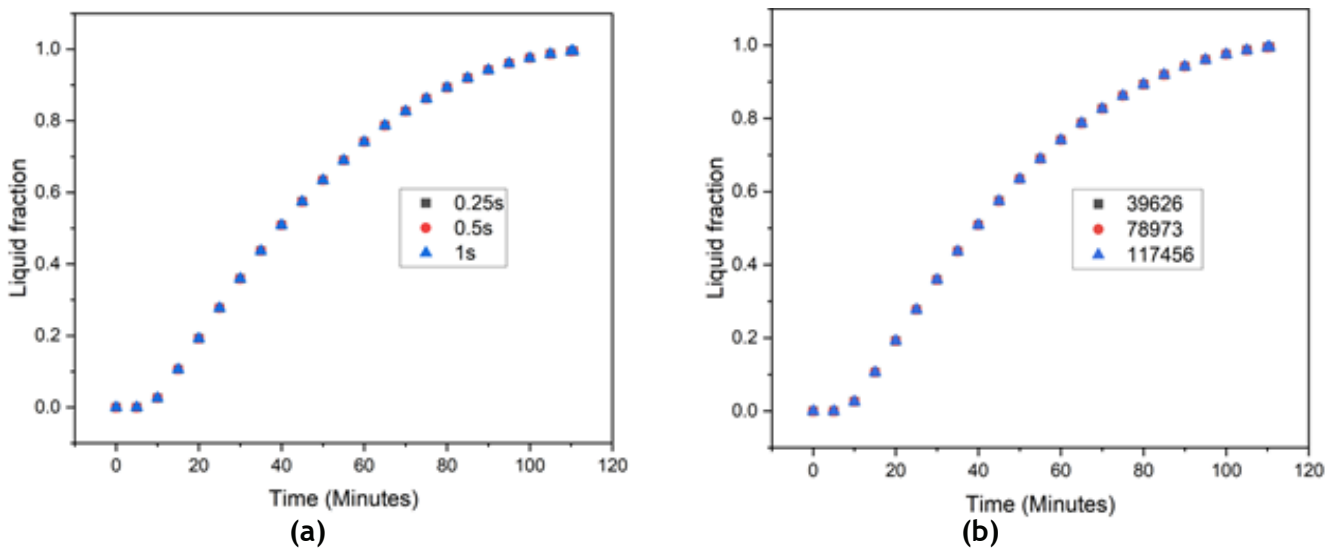

Figure 4. (a) Grid and (b) Time-step independency test against temperature.

transfer of 5kw/m² is provided to the top walls of the heat sink to permit natural cooling. Additionally, Adiabatic boundaries are provided to the side and bottom wall of the heat sink to prevent dissipation of heat from the system.

3.1 Heat Sink Based on Pure PCM

Figure 5 shows the liquid fraction fluctuation when Pure PCM is present (φ= 0%) in the heat sink. The time required to attain the complete charging time at 6 and 7 kW/m² is 119 and 93 minutes, respectively. At 8, 9, and 10 kW/m², the PCM entirely melts in 88, 74, and 63 minutes, respectively. Due to the phase transition that takes place at the boundary between the heater and PCM, intense energy absorption begins virtually simultaneously with melting at values of 7 kW/m² and above. Moreover, a considerable phase change is influenced by an increase in the temperature gradient.

Figure 6 illustrates the heat sink's temperature change. The PCM may reach a maximum temperature of 330 K, 365 K, 370 K, 378 K, and 389 K during a full cycle of charging at 6–10 kW/m² input, respectively. At 6 kW/

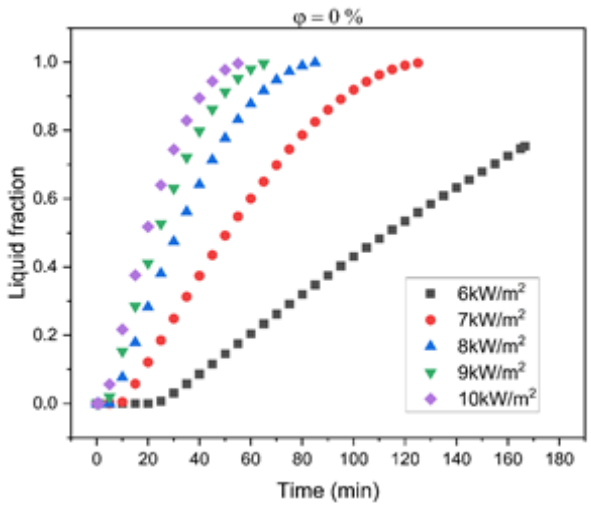

Figure 5. Pure PCM liquid fraction at input heat flux 6 -10 kW/m²

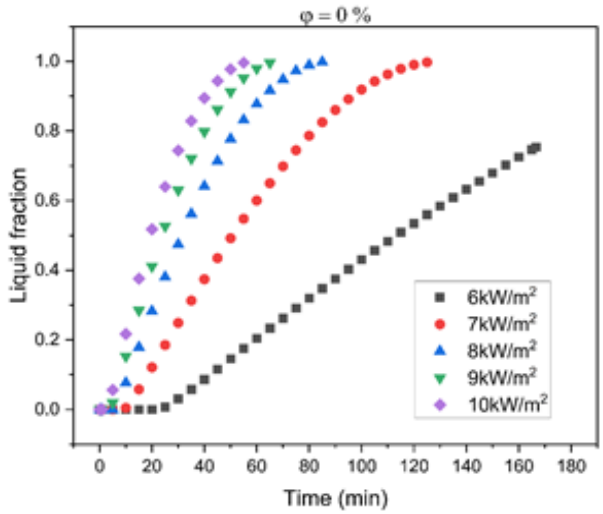

Figure 6. Pure PCM temperature variation at input heat flux 6 -10 kW/m²

m^2, the PCM rapidly increases the temperature to 312 K, then slowly and steadily. In contrast, at 7 kW/m^2, the PCM temperature increases higher than in the earlier scenario. A bigger temperature was gained as a result of the additional heat flux increase.

3.2 NePCM Based Heat Sink

Figure 7 represents the change in melt percentage of the heat sink over time when NePCM is present at volume fraction of φ = 1%, 2%, and 3%. The liquid fraction rises more slowly as nanoparticle concentration rises. The liquid fraction of the material with φ = 0.5% of nanoparticles rises more quickly with a heat flux input of 10 kW/m^2, which is the lone exception. The reduced value of latent heat at lowering nanoparticle concentration in PCM can be used to explain this result.

Figure 8 shows three plots of the NePCM's average temperature variation against time for input heat fluxes between 6 to 10 kW/m^2 and volume fraction φ = 1%, 2%, and 3% nanoparticle concentrations. The temperature range could be separated into three categories, with the first category showing a linear increase in temperature that is abrupt. The temperature increases in the second category, which is quite longer than the first but still apprehends the same pattern. This stage is crucial because a significant portion of its domain melts, slowly raising the melt temperature. In the third category, the entire zone is almost completely melting, and the temperature is swiftly rising again.

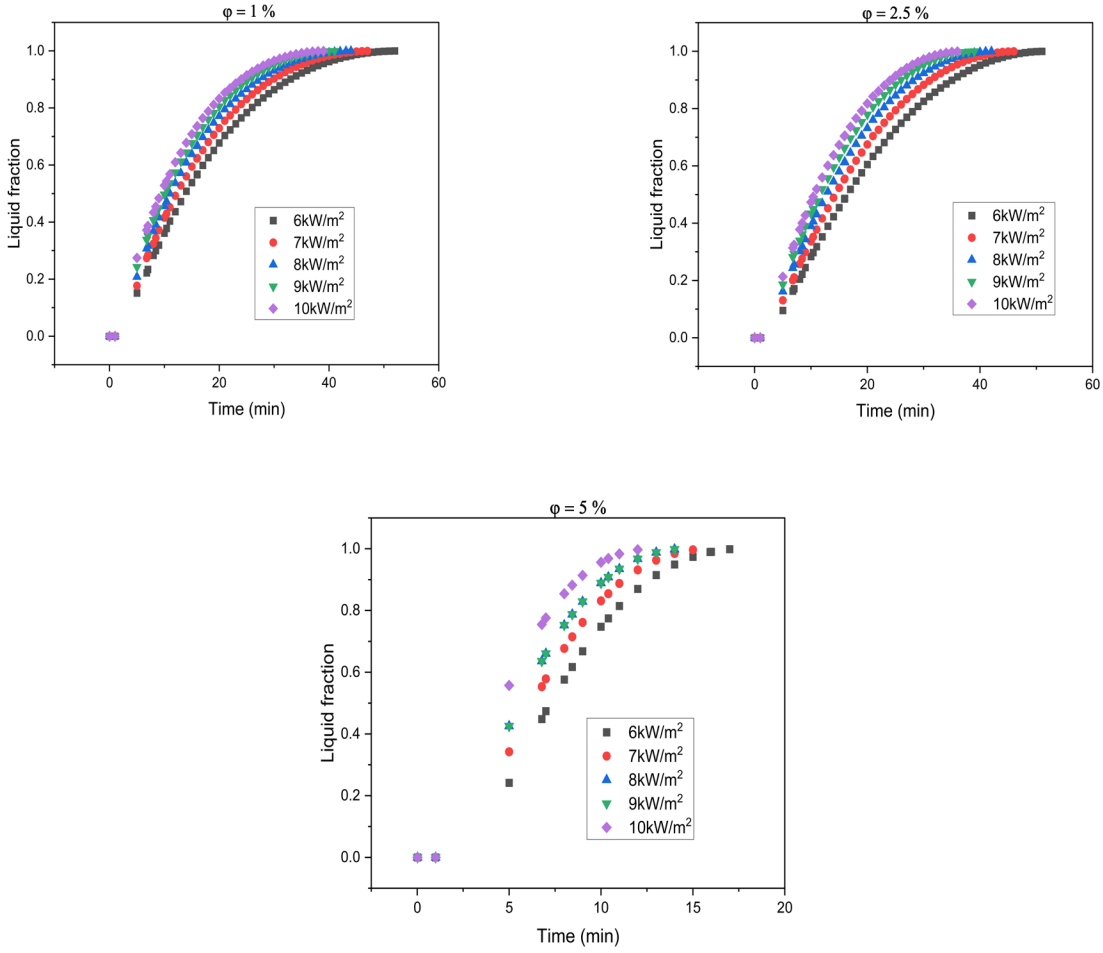

Figure 7. NePCM liquid fraction at input heat flux 6 -10 kW/m^2.

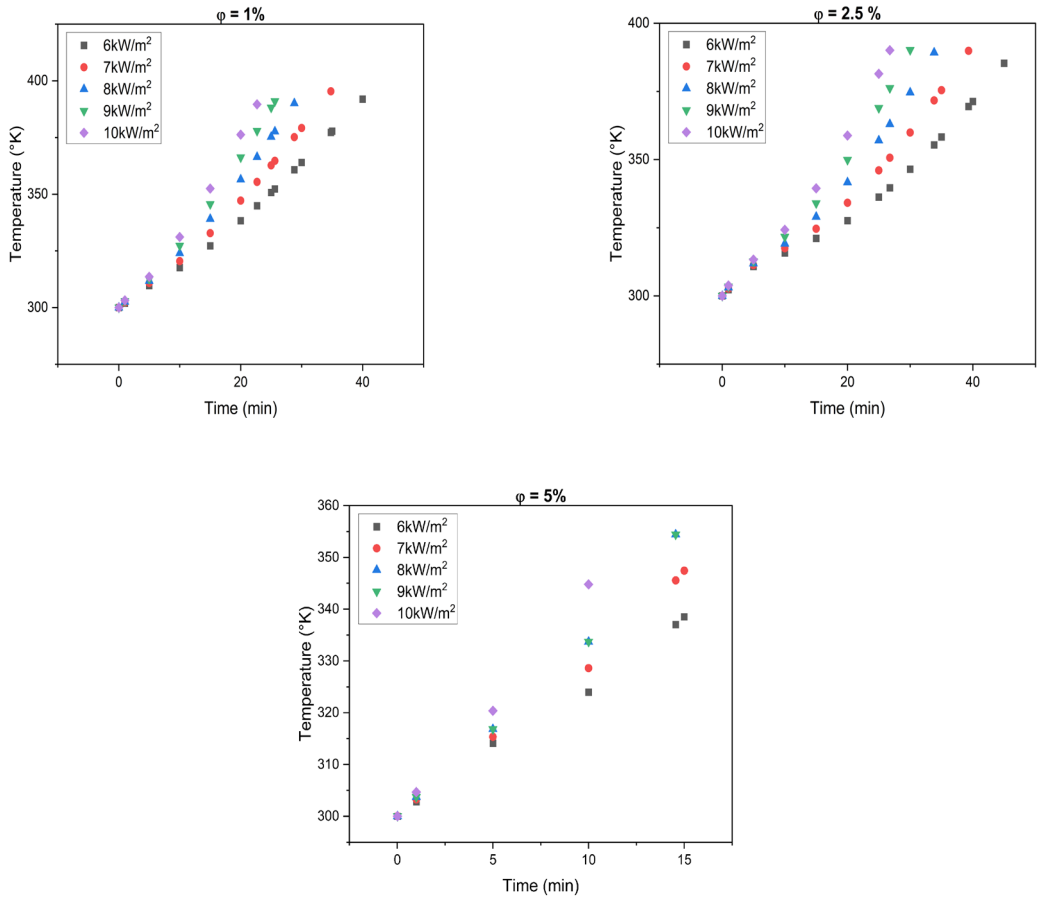

Figure 8. NePCM temperature variation at input heat flux 6 -10 kW/m^2.

3.3 Comparison of Pure PCM and NePCM-Based Heat Sink

Figure 9(a) represents heat-sink charging time against input heat flux. The percentage reduction in charging time of NePCM (φ = 1%, 2.5%, and 5%) in comparison to the pure PCM (φ = 0%) is 69%, 78%, and 88% respectively at 6 kW/m^2 input. The lowest charging time was recognized at φ = 5%. Similarly, for other heat flux ranges (7–10 kW/m^2) a significant reduction in charging time was found at φ = 2.5% and 5% respectively. The temperature distribution against heat flux is represented in Figure 9(b). The temperature reduction percentage of NePCM is 24%, 46%, and 74% respectively against pure PCM for complete charging time at 6kW/m^2 input respectively. This denotes an effective reduction of melting temperature for the complete charging cycle of NePCM. Thus signifying a reduction in temperature resistance and keeping the heat sink well below the critical temperature.

4.0 Conclusion

The numerical analysis presented in this research is centered on the potential usage of Nano-PCM for cooling electronics. Al_2O_3 nanoparticles were seeded into a PCM having a melt temperature of 44°C at volume fractions of 0.5%, 1%, and 2.5%, respectively. To understand how nanoparticles, affect the solid-liquid phase shift process in passive electronics cooling device, transient 3-D numerical simulations of PCM/NePCM-based heat sinks were analyzed at input heat fluxes of 6–10 kW/m^2. The outcomes demonstrate that the Nano-PCMs can delay the melting process with a well-established temperature thus depicting better cooling characteristics.

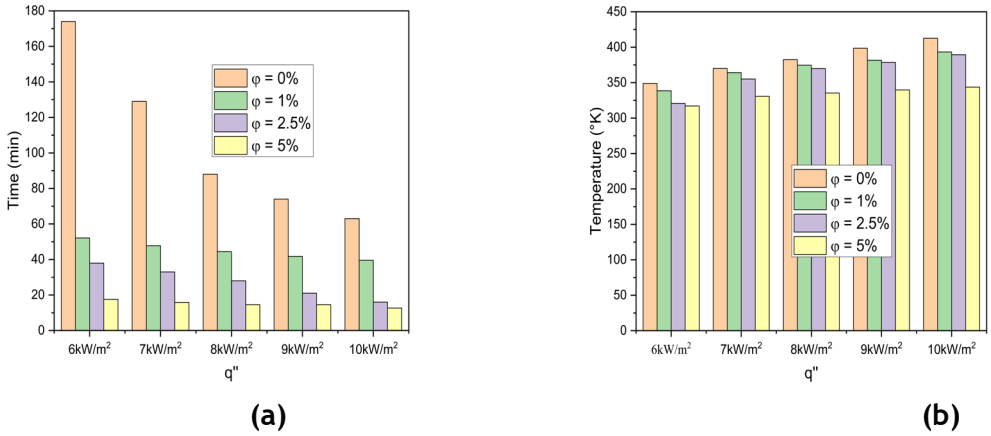

Figure 9. (a) Charging time against input heat flux (b) Charging temperature against input heat flux.

5.0 References

1. Tariq SL, Ali HM, Akram MA, Janjua MM, Ahmadlouydarab M. Nanoparticles enhanced phase change materials (NePCMs)-A recent review. Appl Therm Eng. 2020 April; 176:115305.
2. Alimohammadi M, Aghli Y, Alavi ES, Sardarabadi M, Passandideh-Fard M. Experimental investigation of the effects of using nano/phase change materials (NPCM) as coolant of electronic chipsets, under free and forced convection. Appl Therm Eng. 2017; 111:271–9.
3. Moon H, Miljkovic N, King WP. International Journal of Heat and Mass Transfer High power density thermal energy storage using additively manufactured heat exchangers and phase change material. Int J Heat Mass Transf. 2020; 153:119591.
4. Colla L, Fedele L, Mancin S, Danza L, Manca O. Nano-PCMs for enhanced energy storage and passive cooling applications. Appl Therm Eng. 2017; 110:584–9.
5. Colla L, Fedele L, Mancin S, Buonomo B, Ercole D, Manca O. Nano-PCMs for passive electronic cooling applications. J Phys Conf Ser. 2015; 655(1).
6. Buonomo B, Ercole D, Manca O, Nardini S. Numerical analysis on a latent thermal energy storage system with phase change materials and aluminum foam. Heat Transfer Engineering. 2020 Jul 3; 41(12): 1075–84.
7. Mahdavi M, Tiari S, Pawar V. A numerical study on the combined effect of dispersed nanoparticles and embedded heat pipes on melting and solidification of a shell and tube latent heat thermal energy storage system. J Energy Storage. 2020; 27:101086.
8. Ghalambaz M, Mehryan SAM, Veismoradi A, Mahdavi M, Zahmatkesh I, Kazemi Z, et al. Melting process of the nano-enhanced phase change material (NePCM) in an optimized design of shell and tube thermal energy storage (TES): Taguchi optimization approach. Appl Therm Eng. 2021; 193:116945.
9. Pandiyan PS. Thermal performance assessment of phase change material for electronic cooling: An experimental investigation. 2022 April; 1–10.
10. Brent AD, Voller VR, Reid KJ. Enthalpy-porosity technique for modeling convection-diffusion phase change: application to the melting of a pure metal. Numerical Heat Transfer: An International Journal of Computation and Methodology. 1988 Apr; 13(3):297–318.
11. Ye WB, Zhu DS, Wang N. Numerical simulation on phase-change thermal storage/release in a plate-fin unit. Appl Therm Eng. 2011 Dec; 31(17–18):3871–84.
12. ANSYS. ANSYS Fluent Theory Guide. ANSYS 162 Documentation. 2015 July; 15317:80.
13. Bock Choon Pak Young IC. Hydrodynamic and heat transfer study of dispersed fluids with submicron metallic oxide. Experimental Heat Transfer: A Journal of, Thermal Energy Transport, Storage, and Conversion. 2013 January; 2013:37–41.
14. Vajjha RS, Das DK, Namburu PK. Numerical study of fluid dynamic and heat transfer performance of Al_2O_3 and CuO nanofluids in the flat tubes of a radiator. Int J Heat Fluid Flow. 2010; 31(4):613–21.
15. Krieger IM, Dougherty TJ. A mechanism for non-Newtonian flow in suspensions of rigid spheres. Transactions of the Society of Rheology. 1959; 3(1):137–52.

16. Santamaría-Holek I, Mendoza CI. The rheology of concentrated suspensions of arbitrarily-shaped particles. J Colloid Interface Sci. 2010; 346(1):118–26.
17. Flynn HG. Transport Phenomena. Phys Today. 1962; 15(6):96–8.
18. Haariet Martique. This is a reproduction of a library book that was digitized by Google as part of an ongoing effort to preserve the information in books and make it universally accessible. https://books.google.com. Oxford University. 1994; XXX:60.
19. Arshad A, Ali HM, Khushnood S, Jabbal M. Experimental investigation of PCM based round pin-fin heat sinks for thermal management of electronics: Effect of pin-fin diameter. Int J Heat Mass Transf. 2018; 117:861–72.
20. Ashraf MJ, Ali HM, Usman H, Arshad A. Experimental passive electronics cooling: Parametric investigation of pin-fin geometries and efficient phase change materials. Int J Heat Mass Transf. 2017 Dec 1; 115:251–63.
21. Arshad A, Ali HM, Ali M, Manzoor S. Thermal performance of phase change material (PCM) based pin-finned heat sinks for electronics devices: effect of pin thickness and PCM volume fraction. Appl Therm Eng. 2017 Feb 5; 112:143–55.
22. Ali HM, Arshad A, Jabbal M, Verdin PG. Thermal management of electronics devices with PCMs filled pin-fin heat sinks: A comparison. Int J Heat Mass Transf. 2018; 117(February):1199–204.

Nomenclature:

A_{mush}	Mushy zone constant (kg/m^3 s)
c_p	Specific heat of PCM (J/kg K)
$\vec{F}$	External body forces (N)
g	Gravity acceleration (m /s^2)
h	Sensible enthalpy (J / kg)
H	Enthalpy (J / kg)
K	Thermal conductivity (W /m K)
T	Temperature (°C or K)
$\vec{v}$	Velocity component (m/s)
L	Latent heat fusion (J/kg)
Nu	Nusselt number = (hl)/k
p	Static pressure (N/m^2)
S_i	Momentum source term (Pa/m)

Greek letters

β	Thermal expansion coefficient (K)
γ	Liquid fraction
ρ	Fluid density(kg/m^3)
$\bar{\bar{\tau}}$	Stress tensor (N/m^2)
φ	Nano-additives volume fractions (%)

Subscripts

HTF	Heat transfer fluid
ini	Initial
l	Liquidus of the phase change material
Ref	Reference
s	Solidus of the phase change material

Abbreviations

NePCM	Nano enhanced phase change material
Nm	Nano-materials
NP	Nano-particles
PCM	Phase change materials
LHTES	Latent heat thermal storage system